Available online at www.sciencedirect.com

SciVerse ScienceDirect

Ceramics International 39 (2013) S555–S558

CERAMICS INTERNATIONAL

www.elsevier.com/locate/ceramint

Effects of barium on luminescent properties of $Sr_{2-x}Ba_xSiO_4:Eu^{2+}$ nanoparticles

Jun Seong Lee, Young Jin Kim*

Department of Materials Science and Engineering, Kyonggi University, Suwon 443-760, Republic of Korea

Available online 17 October 2012

Abstract

$Sr_{2-x}Ba_xSiO_4:Eu^{2+}$ nanopowders were synthesized by a co-precipitation method using alkaline earth metal nitrates, europium nitrate hydrate, and 3-aminopropyltriethoxysilane (APTES) as starting materials. The substitution of Ba^{2+} ions for Sr^{2+} ions caused the phase transition from β- to α′-Sr_2SiO_4. SEM micrographs exhibited uniform anisotropic nanoparticles with high aspect ratios. The photoluminescence (PL) excitation spectra of $Sr_{2-x}Ba_xSiO_4:Eu^{2+}$ consisted of two bands originated from Eu(I) and (II) sites, respectively, resulting in two corresponding emission bands at around 473 and 543 nm. The PL spectra exhibited the red- or blue-shift of dominant emission wavelengths, depending on the Ba^{2+} content.

Keywords: A. Powders: chemical preparation; C. Optical properties; D. Alkaline earth oxides; D. Silicate

1. Introduction

Alkaline earth metal silicate powders are excellent phosphors for white light emitting diodes (WLEDs) and electronic displays. At present, yellow emitting $Y_3Al_5O_{12}:Ce^{3+}$ (YAG:Ce^{3+}) phosphors are commercially combined with blue LED chips for WLEDs [1–3].

Eu^{2+} doped strontium orthosilicate ($Sr_2SiO_4:Eu^{2+}$) is one of the prevailing green–yellow phosphors for WLEDs due to its excellent luminescent properties. Several synthesizing methods have been suggested: a conventional solid-state reaction [4–6] and chemical preparation methods [7,8]. Sr_2SiO_4 has two polymorphs of the low temperature β-form (monoclinic) and high temperature α′-form (orthorhombic). There are two alkaline earth metal sites in M_2SiO_4: ten-coordinated M(I) and nine-coordinated M(II) by oxygen atoms [9], leading to two emission bands at around 480 nm and 560 nm assigned to Eu(I) and (II), respectively [4,5]. On the other hand, it was reported that two emission peaks of $Ba_2SiO_4:Eu^{2+}$ overlapped to result in a single band at around 500 nm [5]. Ba_2SiO_4 is orthorhombic and isostructural with β-K_2SO_4 [10].

The luminescent properties of binary alkaline earth orthosilicate $(M,M')_2SiO_4$ powders are reported that their optical properties depend on the cation ratios of M/M′, a flux, co-doping materials, etc. [10–14].

In this work, $Sr_{2-x}Ba_xSiO_4:Eu^{2+}$ nanopowders were prepared by a co-precipitation method, and then the effects of Ba^{2+} ions on the structural and luminescent properties were investigated.

2. Experimental

$Sr_{2-x}Ba_xSiO_4:0.005Eu^{2+}$ nanopowders were prepared by a co-precipitation method using $Sr(NO_3)_2$ (Sigma Aldrich, 99.995%), $Ba(NO_3)_2 \cdot xH_2O$ (Sigma Aldrich, 99.999%), $Eu(NO_3)_3 \cdot xH_2O$ (Sigma Aldrich, 99.99%), and $H_2N(CH_2)_3Si(OC_2H5)_3$ (APTES; Sigma Aldrich, ≥98%) as starting materials. (0.2 M) of $Sr(NO_3)_2$, $Ba(NO_3)_2$, and $Eu(NO_3)_3$ were dissolved in deionized water, and then their solutions were stoichiometrically mixed in Teflon beakers. Meanwhile, 0.5 M APTES was dissolved in ethanol and injected dropwise into the mixed nitrate aqueous solution. This solution was held for 24 h at room temperature for the slow precipitation reaction. As-prepared precipitates were washed, mixed with a flux of 2 wt% NH_4Cl, and then fired at 1300 °C for 5 h under 5%

*Corresponding author. Tel.: +82 31 249 9766; fax: +82 31 244 6300.
E-mail address: yjkim@kyonggi.ac.kr (Y.J. Kim).

0272-8842/$ - see front matter © 2012 Elsevier Ltd and Techna Group S.r.l. All rights reserved.
http://dx.doi.org/10.1016/j.ceramint.2012.10.134

H_2 (95% N_2) atmosphere in an electric tube furnace for the reduction process of $Eu^{3+} \rightarrow Eu^{2+}$.

An X-ray diffractometer (XRD, Rigaku, Miniflex II) using Cu K_α radiation ($\lambda = 1.5406$ Å) was used to determine the crystal structure. The particle size and morphology were observed by a field-emission scanning electron microscope (FESEM, JEOL, JSM-6700F). The photoluminescence (PL) spectra were measured by a PL system (PSI, Darsa-5000) with a 500 W xenon lamp.

3. Results and discussion

The structural dependence of $Sr_{2-x}Ba_xSiO_4:Eu^{2+}$ (SBSO: Eu^{2+}, $0 < x < 2$) nanopowders on the Ba content was investigated by XRD as shown in Fig. 1. At $x=0$, XRD peaks of $Sr_2SiO_4:Eu^{2+}$ (SSO:Eu^{2+}) just corresponded to JCPDS data (38-0271) of the low temperature β-SSO phase (monoclinic). On the other hand, at $x=0.1$ the β-SSO phase was completely transformed into the pure α′-SSO phase. XRD patterns of α-SSO and β-SSO are very similar to each other, because the $\beta \leftrightarrow \alpha'$ transformation is displacive. Therefore, each phase can be identified by comparing their distinctive XRD peaks, which are marked with α′ and β. It was suggested that the substitution of a small amount of Ba^{2+} ions for Sr^{2+} ions of β-SSO could cause the transformation from β- to α′-form even at room temperature, even though the α′-SSO phase could not be quenched to room temperature [4,15]. With the increase in the Ba content ($0.1 < x < 2.0$), the XRD peaks of the SBSO solid solution continuously moved toward the lower angles (Fig. 1(b)–(h)), and finally they coincided with those of the orthorhombic BSO phase at $x=2$ (Fig. 1(i)). These shift of XRD peaks were attributed to different ionic size between Sr^{2+} (1.31/1.36 Å for coordination number (CN)=9/10) and Ba^{2+} (1.47/1.52 Å for CN=9/10) ions. Compared with Sr^{2+} ions, the larger substituted Ba^{2+} ions extended the lattice parameters, and so the representative XRD peaks of α-SSO (marked as α′ at $2\theta = 27.199°$) apparently shifted to the lower angles.

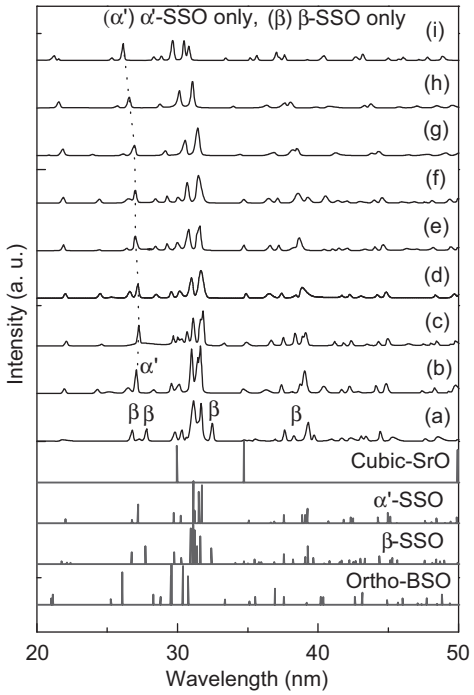

Fig. 1. XRD patterns of $Sr_{2-x}Ba_xSiO_4:Eu^{2+}$ powders. (a) $x=0$, (b) $x=0.1$, (c) $x=0.2$, (d) $x=0.3$, (e) $x=0.4$, (f) $x=0.5$, (g) $x=1.0$, (h) $x=1.5$, and (i) $x=2.0$.

SEM micrographs of $Sr_{2-x}Ba_xSiO_4:Eu^{2+}$ ($x=0-2.0$) powders are shown in Fig. 2(a)–(i). Pure β-SSO powders were composed of nanoparticles with high aspect ratios (L/D, L: length; D: diameter). The diameter (D) ranges about 50–100 nm. This anisotropic growth was attributed to the preferential binding of reactants to a specific crystal plane, and this behaviour was closely correlated with the surface free energy and the surface area of growing crystals. With increasing Ba^{2+} content up to $x=1.5$ the particle size slightly increased, thereafter it significantly shortened at $x=2.0$ as shown in Fig. 2(i).

For comparison, the PL excitation (PLE) spectra of SSO:Eu^{2+}, $SrBaSiO_4:Eu^{2+}$, and BSO:Eu^{2+} are shown in Fig. 3. The PLE spectrum of SSO:Eu^{2+} exhibits two peaks at around 330 (A-band) and 375 nm (B-band). They are assigned to two different activation centers: Eu(I) and (II) sites. The B-band is much higher than the A-band, because that is more favorable for the 543 nm emission. In the case of $SrBaSiO_4:Eu^{2+}$, the distinction between the A- and B-bands became smaller due to the incorporation of the Ba^{2+} ions as shown in Fig. 3(b), while both bands almost overlapped for BSO:Eu^{2+}.

Fig. 4 depicts the PL spectra of $Sr_{2-x}Ba_xSiO_4:Eu^{2+}$ powders that are excited by the A- (left) and B-bands (right), respectively. The PLE and PL spectra of SSO:Eu^{2+} nanoparticles in this work were well matched with

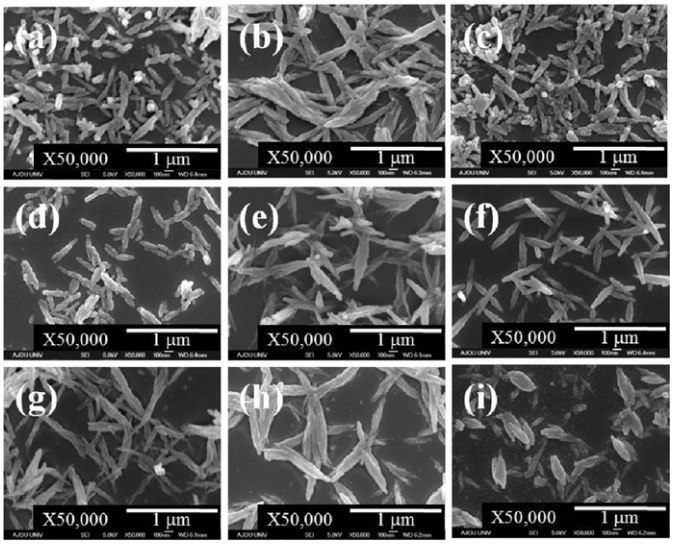

Fig. 2. SEM micro-graphs of $Sr_{2-x}Ba_xSiO_4:Eu^{2+}$ powders. (a) $x=0$, (b) $x=0.1$, (c) $x=0.2$, (d) $x=0.3$, (e) $x=0.4$, (f) $x=0.5$, (g) $x=1.0$, (h) $x=1.5$, and (i) $x=2.0$.

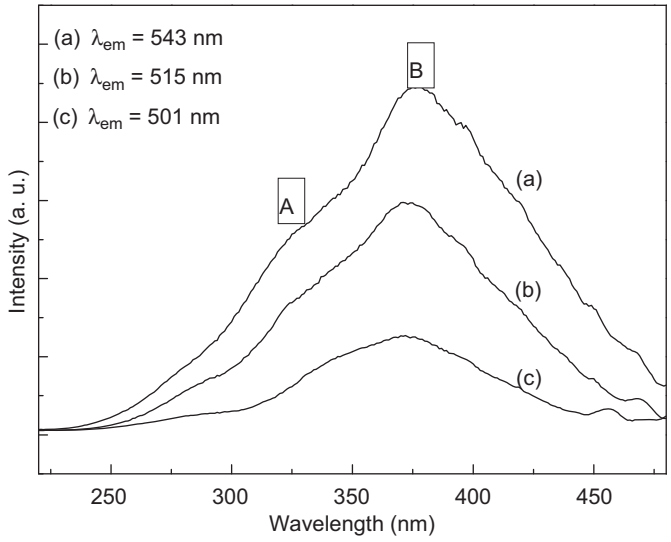

Fig. 3. The PLE spectra of (a) Sr_2SiO_4:Eu^{2+}, (b) $SrBaSiO_4$:Eu^{2+}, and (c) Ba_2SiO_4:Eu^{2+}.

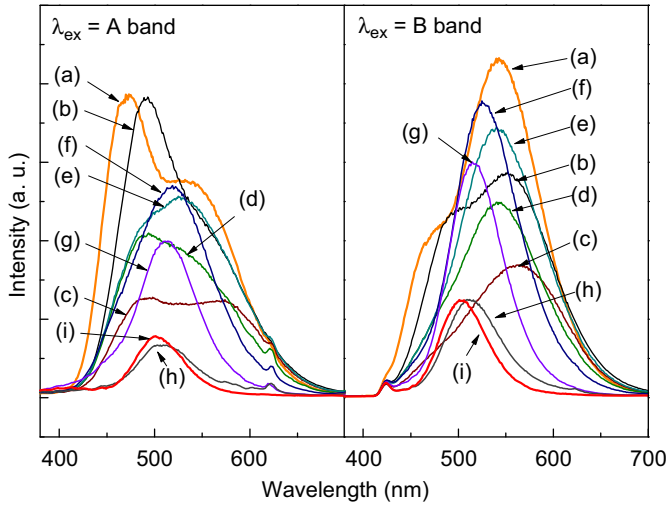

Fig. 4. The emission spectra of $Sr_{2-x}Ba_xSiO_4$:Eu^{2+} powders. (a) $x=0$, (b) $x=0.1$, (c) $x=0.2$, (d) $x=0.3$, (e) $x=0.4$, (f) $x=0.5$, (g) $x=1.0$, (h) $x=1.5$, and (i) $x=2.0$ (left: λ_{ex}=A band, right: λ_{ex}=B band).

those of SSO:Eu^{2+} powders prepared by a conventional solid-state reaction method [5]. Pure SSO:Eu^{2+} powders have two emission bands at around 475 and 535 nm dominantly assigned to Eu(I) and (II), respectively, because the crystal fields surrounding Eu(II) sites (CN=9) are stronger than those surrounding of Eu(I) sites (CN=10) due to shorter bond lengths of Eu–O [4]. The 473 nm and 543 nm emissions were dominant emission wavelengths under the A- and B-bands excitations, respectively. This revealed that the A- and B-bands are favourable for the Eu(I) and Eu(II) activation, respectively. With increasing Ba content (x) the PL spectra significantly changed under both A- and B-bands excitations. This spectral evolution was very complicated, and it could be

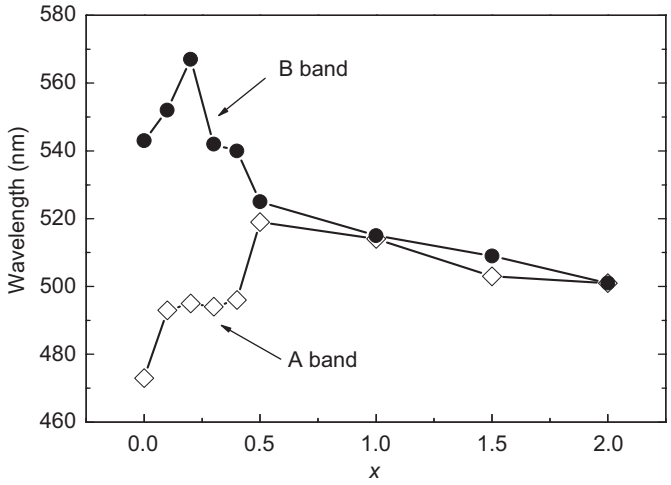

Fig. 5. The variation of the dominant wavelength of $Sr_{2-x}Ba_xSiO_4$:Eu^{2+} powders. (a) λ_{ex}=330 nm and (b) λ_{ex}=375 nm.

explained by the interference between two emission bands due to the Eu(I) and Eu(II) sites. The substitution of Ba^{2+} ions caused the change of the crystal field surrounding Eu^{2+} ions, and its influence was different at the Eu(I) and Eu(II) sites, leading to the distinctive variation of the PL intensity and the emission wavelength at each site. This is described in Fig. 5. Finally, two emission peaks of BSO:Eu^{2+} overlapped to be a single band at around 500 nm [5].

Meanwhile, at $x=0.1-1.5$, weak red emissions at around 622 nm were observed under A-band excitation, but not under B-band excitation. On the other hand, they were not detected for SSO: Eu^{2+} ($x=0$) and BSO:Eu^{2+} ($x=2$). These red emissions were possibly ascribed to the SrO:Eu^{2+} phase, because SrO:Eu^{2+} powders, which were prepared in this work, exhibited red emission bands at around 616 nm under 300 nm excitation. The previous work also reported the red emission of SrO:Eu^{2+} [16]. These findings corresponded to Fig. 1 where insignificant SrO XRD peaks were observed.

The dominant peak wavelength (DPW) of the emission spectra of $Sr_{2-x}Ba_xSiO_4$:Eu^{2+} was closely correlated with x values as shown in Fig. 5(a) and (b). Under A-band excitations, the increase in the Ba content ($x=0-0.5$) caused DPW to continuously shift to longer wavelengths (red-shift), whereas the blue-shift was observed at $x=1.0-2.0$. When excited by the B-band, the large red-shift was attained up to $x=0.2$, but further increase ($x=0.3-2.0$) resulted in the blue-shift. A crystal field strength is related with ionic size by the equation of $Dq \sim R^{-5}$, where Dq is the crystal field strength and R is the bond length between a centre ion and ligand ions (M–O) [17]. Consequently, the substitution of large Ba^{2+} ions for Sr^{2+} ions had to reduce the crystal field strength to result in the blue-shift of SBO:Eu^{2+} powders with increasing Ba^{2+} content (x). These unexpected red-shifts at the low Ba^{2+} concentration can be explained by considering two factors: the covalence and the crystal field strength. In

case of the B-band excitation in Fig. 5(b), at the low content of Ba^{2+} ions ($x=0-0.2$) the effects of the degree of covalence, which increased by substituting Sr^{2+} ions with large Ba^{2+} ions, were superior to those of the weakened crystal field strength due to large Ba^{2+} ions, leading to the red-shift. On the contrary, at more than $x=0.2$, the ionic size effects surpassed the contribution of the covalence because of the high concentration of Ba^{2+} ions, resulting in the blue-shift. Meanwhile, under A-band excitation, DPW exhibited the red-shift at $x=0-0.5$, whereas the higher x values ($x>0.5$) led to the blue-shift (Fig. 5(a)) in the same way with the B-band excitation. However, the Ba content for the change from the red- to blue-shifts of DPW was larger under A-band excitation ($x=0.5$) than under B-band excitation ($x=0.2$). DPWs are dominantly attributed to Eu(I) and (II) sites under A- and B-band excitation, respectively. Meanwhile, the length of Eu–O bond at the Eu(I) site is longer than that at the Eu(II) site due to the larger CN, and so the crystal field strength effects under A-band excitation were predominant at higher x value than those under B-band excitation.

4. Conclusions

The substitution of Ba^{2+} ions for Sr^{2+} of β-SSO:Eu^{2+} powders resulted in the α-SBSO solid solutions, whose XRD peaks moved toward the lower angles due to the large Ba^{2+} ions. The powders consisted of nanoparticles with high aspect ratios due to the anisotropic growth. SBSO:Eu^{2+} powders exhibited the red- or blue-shift, depending on the Ba^{2+} content and excitation wavelengths.

Acknowledgements

This work was supported by Basic Science Research Program through the National Research Foundation of Korea (NRF) funded by the Ministry of Education, Science and Technology (2010-0008994).

References

[1] K. Bando, K. Sakano, Y. Noguchi, Y. Shimizu, Development of high-bright and pure-white LED lamps, Journal of Light & Visual Environment 22 (1998) 2–5.

[2] Y. Pan, M. Wu, Q. Su, Comparative investigation on synthesis and photoluminescence of YAG:Ce phosphor, Materials Science and Engineering B 106 (2004) 251–256.

[3] S. Nishiura, S. Tanabe, K. Fujioka, Y. Fujimoto, M. Nakatsuka, Preparation and optical properties of transparent Ce:YAG ceramics for high power white LED, IOP Conference Series Materials Science and Engineering. 1 (2009) 012031–012035.

[4] J.H. Lee, Y.J. Kim, Photoluminescent properties of Sr_2SiO_4:Eu^{2+} phosphors prepared by solid-state reaction method, Materials Science and Engineering B 146 (2008) 99–102.

[5] H. Guo, X.F. Wang, X.B. Zhang, Y.F. Tang, L.X. Chen, C.G. Ma, Effect of NH_4F flux on structural and luminescent properties of Sr_2SiO_4:Eu^{2+} phosphors prepared by solid-state reaction method, Journal of the Electrochemical Society 157 (8) (2010) J310–J314.

[6] S.H.M. Poort, W. Janssen, G. Blasse, Optical properties of Eu^{2+}-activated orthosilicates and orthophosphates, Journal of Alloys and Compounds 260 (1997) 93–97.

[7] W.H. Hsu, M.H. Sheng, M.S. Tsai, Preparation of Eu-activated strontium orthosilicate ($Sr_{1.95}SiO_4$:$Eu_{0.05}$) phosphor by a sol–gel method and its luminescent properties, Journal of Alloys and Compounds 467 (2009) 491–495.

[8] B. Lei, K.I. Machida, T. Horikawa, H. Hanzawa, Facile combustion route for low-temperature preparation of Sr_2SiO_4:Eu^{2+} phosphor and its photoluminescence properties, Japanese Journal of Applied Physics 49 (2010) 095001–095006.

[9] M. Catti, G. Gazzoni, G. Ivaldi, Structures of twinned β-Sr_2SiO_4 and of α′-$Sr_{1.9}Ba_{0.1}SiO_4$, Acta Crystallographica Section C 39 (1983) 29–34.

[10] J.S. Kim, P.E. Jeon, J.C. Choi, H.L. Park, Emission color variation of M_2SiO_4:Eu^{2+} (M=Ba, Sr, Ca) phosphors for light-emitting diode, Solid State Communications 133 (2005) 187–190.

[11] J.S. Kim, Y.H. Park, J.C. Choi, H.L. Park, Optical and structural properties of Eu^{2+}-doped $(Sr_{1-x}Ba_x)_2SiO_4$ phosphors, Journal of the Electrochemical Society 152 (9) (2005) H135–H137.

[12] H.S. Kang, Y.C. Kang, K.Y. Jung, S.B. Park, Eu-doped barium strontium silicate phosphor particles prepared from spray solution containing NH_4Cl flux by spray pyrolysis, Materials Science and Engineering B 121 (2005) 81–85.

[13] H.S. Kang, S.K. Hong, Y.C. Kang, K.Y. Jung, Y.G. Shul, S.B. Park, The enhancement of photoluminescence characteristics of Eu-doped barium strontium silicate phosphor particles by co-doping materials, Journal of Alloys and Compounds 402 (2005) 246–250.

[14] P. Dorenbos, Energy of the first $4f^7 \rightarrow 4f^65d$ transition of Eu^{2+} in inorganic compounds, Journal of Luminescence 104 (2003) 239–260.

[15] G. Pieper, W. Eysel, Th. Hahn, Solid solubility and polymorphism in the system Sr_2SiO_4–Sr_2GeO_4–Ba_2GeO_4–Ba_2SiO_4, Journal of the American Ceramic Society 55 (1972) 619–622.

[16] N. Yamashita, Photoluminescence spectra of the Eu^{2+} center in SrO:Eu, Journal of Luminescence 59 (1994) 195–199.

[17] S. Perkowitz, Optical Characterization of Semiconductors: Infrared, Raman, and Photoluminescence Spectroscopy, Academic Press, New York, 1993.